# A high-contrast imaging survey of nearby red supergiants

## Peter Scicluna[1], Ralf Siebenmorgen[2], Joris Blommaert[3], Francisca Kemper[1], Roger Wesson[4] and Sebastian Wolf[5]

[1]Academia Sinica, Institute of Astronomy and Astrophysics, 11F Astronomy-Mathematics Building, NTU/AS campus, No. 1, Section 4, Roosevelt Rd., Taipei 10617, Taiwan, Republic of China
email: peterscicluna@asiaa.sinica.edu.tw

[2]European Southern Observatory, Karl-Schwarzschild-Str. 2, 85748, Garching b. München, Germany

[3]Astronomy and Astrophysics Research Group, Dep. of Physics and Astrophysics, V.U. Brussel, Pleinlaan 2, 1050, Brussels, Belgium

[4]Dept. of Physics & Astronomy, University College London, Gower Street, London WC1E 6BT, UK

[5]Institute of Theoretical Physics and Astrophysics, Universität zu Kiel, Leibnizstr. 15, 24118, Kiel, Germany

**Abstract.** Mass-loss in cool supergiants remains poorly understood, but is one of the key elements in their evolution towards exploding as supernovae. Some show evidence of asymmetric mass loss, discrete mass-ejections and outbursts, with seemingly little to distinguish them from more quiescent cases. To explore the prevalence of discrete ejections and companions we have conducted a high-constrast survey using near-infrared imaging and optical polarimetric imaging of nearby southern and equatorial red supergiants, using the extreme adaptive optics instrument SPHERE, which was designed to image planets around nearby stars. We present the initial results of this survey, including the detection of large (500 nm) dust grains in the ejecta of VY CMa and a candidate dusty torus aligned with the maser ring of VX Sgr. We briefly speculate on the consequences for our understanding of mass loss in these extreme stars.

**Keywords.** stars: individual (VY CMa, VX Sgr), stars: mass loss, supergiants

## 1. Introduction

After massive stars ($M > 8\ M_\odot$) leave the main sequence, they undergo periods of enhanced mass loss before exploding as supernovae. This mass loss is a key factor in determining the evolution of the stars through phases including Red Supergiant (RSG), Yellow Hypergiant (YHG), Luminous Blue Variable (LBV), and Wolf-Rayet (WR) (Georgy *et al.* 2013; Smith 2014; Meynet *et al.* 2015; Georgy & Ekström 2015). A proper understanding of mass loss is therefore crucial for determining the post-main sequence evolution of massive stars and for linking classes of supernova progenitors to classes of supernovae, which remains as yet poorly understood (Georgy 2012; Groh *et al.* 2013; Ekström *et al.* 2013; Georgy *et al.* 2013; van Loon 2013).

For stars with initial masses $\lesssim 30\,M_\odot$, a large fraction of the mass loss occurs during the RSG phase. The mechanisms driving mass-loss in this phase remain a matter of debate (van Loon *et al.* 2005; Harper *et al.* 2009), in particular the origins of mass-loss asymmetries, variability and eruptions. Various mechanisms, which may not necessarily be independent, have been invoked, including non-radial pulsations, convection, binarity, and magnetic activity (e.g. Smith *et al.* 2001; Humphreys *et al.* 2007).

However, RSGs are, by definition, bright targets, and answering these questions requires high dynamic range and high angular resolution, while avoiding saturation, if the ejecta is to be separated from the central source. Numerous advances in high-contrast imaging have been driven by the need to image and characterise extrasolar planets, culminating in the development of "extreme adapative optics" (XAO) instruments, such as SPHERE (Beuzit *et al.* 2008), GPI (Macintosh *et al.* 2006) and SCExAO (Martinache & Guyon 2009), which combine coronography with a variety of differential-imaging techniques to achieve contrasts as high as $10^{-7}$ within $0\rlap{.}''5$.

Answering outstanding questions regarding mass-loss from evolved massive stars requires a systematic approach, in which a large sample of supernova progenitors are homogeneously analysed. Hence, we are conducting a high contrast imaging and polarimetry survey of nearby southern and equatorial evolved massive stars, primarily red supergiants, exploiting the capabilities of the new high-contrast, planet-hunting instrument SPHERE, some initial findings from which are included here.

## 2. Target selection

Our target selection is limited by two criteria. First, the extreme adaptive optics (XAO) exploited by modern high-contrast imagers require very bright central point sources to use as natural guide stars (NGS) for optimal AO correction. In the case of SPHERE, the AO correction begins to degrade for NGS with $m_{\rm R} > 9$. The instrument is only available in Service Mode for NGS with $m_{\rm R} \lesssim 11$ which provides high Strehl under a wide range of conditions, although it has been demonstrated that the system operates successfully with an improvement in Strehl for stars as faint as $m_{\rm R} \approx 14$ (Xu *et al.* 2015). Secondly, we require targets sufficiently close to be able to resolve structures in the circumstellar envelope with SPHERE. Given the luminosities of red and yellow supergiants, these criteria restrict us to Galactic sources on low-extinction lines-of-sight, typically within a few kpc or in nearby OB associations.

We therefore selected a sample of 18 bright galactic RSGs to observe with SPHERE, from the spectroscopically confirmed samples of Levesque *et al.* (2005) and Verhoelst *et al.* (2009), focusing on those whose 2MASS and IRAS photometry indicate excess emission, while four additional YHGs were selected based on literature searches. These targets cover a range of luminosities and mass-loss rates to ensure that we sample a useful amount of parameter space.

## 3. Optical Imaging Polarimetry of VY CMa and VX Sgr

### 3.1. *Grain sizes in VY CMa*

In Scicluna *et al.* (2015) we demonstrated some techniques for the survey on the archetypal extreme RSG VY CMa, and we summarise the results here. VY CMa was observed in December 2014 using SPHERE/ZIMPOL in active polarisation compensation mode with fast polarisation modulation. We used V- and I-band filters with a classical Lyot coronagraph to suppress the core of the PSF. The data were reduced using the pipeline to yield reduced images for the Stokes' I, Q and U components for each detector in each filter. These data were combined using python to produce total intensity, linearly-polarised intensity and polarisation angle for each filter.

Figure 1 shows the images obtained in both polarised and unpolarised light. The polarisation images show a clear centro-symmetric pattern, indicating that the polarisation is caused by the scattering of light by dust grains. As a result, we can use the fractional
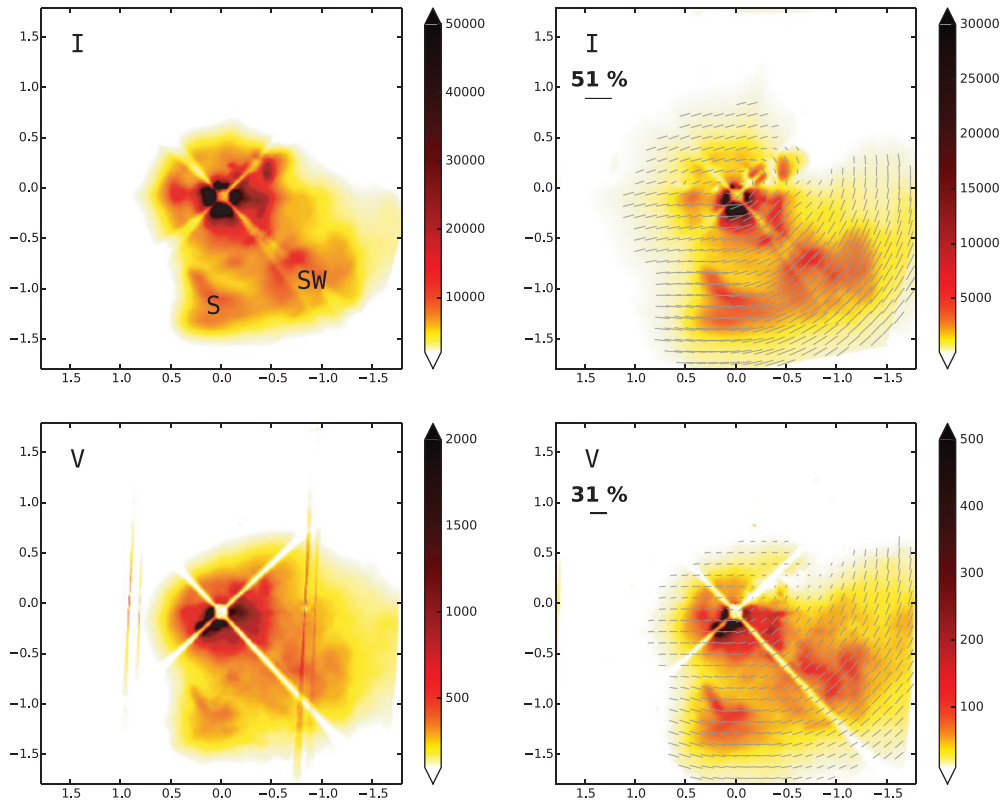
**Figure 1.** SPHERE observations of VY CMa based on Scicluna *et al.* (2015), with offsets in arc seconds and intensity scale in arbitrary units. *Left*: Total intensity. The locations of the South Knot and Southwest Clump are marked with 'S' and 'SW' respectively. The vertical stripes visible in the V-band data are a detector artifact resulting from the readout mode that cancels out in the polarisation data. *Right*: Polarised intensity. The overlaid vectors show the polarisation fraction and direction.

polarisation and the intensity ratio to constrain the properties of the scattering dust, in particular the size distribution of the grains. The very high maximum polarisation degree ($\sim 50\%$) indicates the presence of grains with radii similar to the wavelength of the observations ($\geqslant 100\,\mathrm{nm}$), so we calculate the maximum likelihood values of the minimum ($a_{\min}$) and maximum ($a_{\max}$) radii for an MRN-like grain size distribution (Mathis *et al.* 1977), assuming oxygen-deficient silicates (Ossenkopf *et al.* 1992). To improve the constraints, we also incorporate the published H$\alpha$–polarisation measurements of Jones *et al.* (2007).

We performed detailed fits to two regions of the ejecta, the South Knot and the Southwest Clump, whose 3D positions and motions are known (Humphreys *et al.* 2007). We calculated a grid of grain-size distributions to find maximum likelihood values of $a_{\min}$ and $a_{\max}$ over a relevant parameter space. For the South Knot, a number of good solutions exist for $a_{\min} \geqslant 0.25\,\mu\mathrm{m}$ with $a_{\max}$ only slightly larger than $a_{\min}$, i.e. approximately monodisperse. The best solution lies at $a_{\min} = 0.55\,\mu\mathrm{m}$ and $a_{\max} = 0.58\,\mu\mathrm{m}$, with an average size $\int a n(a)\mathrm{d}a/\int a\mathrm{d}a = \langle a \rangle = 0.56\,\mu\mathrm{m}$. The Southwest Clump shows similar behaviour. However with the maximum likelihood model ($a_{\min} = 0.38\,\mu\mathrm{m}$, $a_{\max} = 0.48\,\mu\mathrm{m}$, average $0.42\,\mu\mathrm{m}$) requires a broader range of grain sizes.
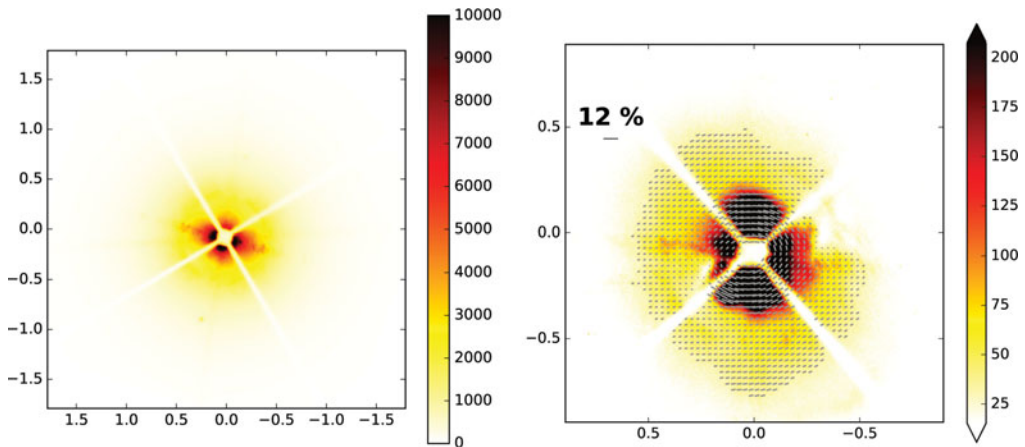
**Figure 2.** SPHERE observations of VX Sgr at 820 nm, with offsets in arcseconds. *Left*: Total intensity, which is likely dominated by the halo resulting from the imperfect AO correction. *Right*: Polarised intensity, zoomed to show only the central arc second.

Although grains larger than $0.1\,\mu$m have been suggested to explain a number of observations of RSGs and of VY CMa in particular, these observations directly confirm grains in this size range, approximately 50 times larger than the average size of interstellar medium (ISM) dust (Mathis *et al.* 1977). As RSGs emit the bulk of their radiation at wavelengths of a few micron, sub-micron dust grains can receive a significant amount of radiation pressure by scattering, rather than absorbing, the stellar emission (Höfner 2008; Bladh & Höfner 2012). This has been found to be an effective mechanism for driving mass loss in oxygen-rich AGB stars (Norris *et al.* 2012), and further work exploring the role of these grains in RSGs will be valuable (e.g. Haubois *et al.*, this volume).

### 3.2. *Morphology of VX Sgr*

VX Sgr was observed on 2015-09-11 with ZIMPOL, using V-band and 820 nm narrowband filters. These data were reduced using the same procedure as the data for VY CMa, and the data for the 820 nm filter are shown in Fig. 2.

The total intensity shows little structure, with most of the emission probably arising from the stellar PSF and imperfect AO correction. However, the polarisation data clearly detects extended structure in the circumstellar shell for the first time. The polarisation vectors produce a clear centro-symmetric pattern with polarisation fraction of several per cent, which, although not conclusive alone, is characteristic of scattering from a dusty circumstellar disc or torus seen nearly face on.

SiO maser emission at 7 mm clearly traces a ring on 1-10 mas scales (Su *et al.* 2012); the coherent velocity structure of this ring is suggestive of an equatorial outflow within 3 R$_{\star}$ seen pole-on. This aligns with the expected location of the inner radius of the candidate disc. Such a torus, however, is difficult to explain without invoking either rapid rotation or the presence of a companion. No point-like sources are visible in our images and the interferometric imaging from Chiavassa *et al.* (2010) did not reveal close-in companions, while hot companions would be obvious from their photospheric spectral signatures. On the other hand, if a companion had previously been accreted it might have spun the star up, providing the necessary rotational energy to eject or form a torus (e.g. Collins *et al.* 1999).

# References

Beuzit, J.-L., *et al.*, 2008, in Ground-based and Airborne Instrumentation for Astronomy II. p. 701418, doi:10.1117/12.790120

Bladh, S., Höfner S., 2012, *A&A*, 546, A76

Chiavassa, A., *et al.*, 2010, *A&A*, 511, A51

Collins, T. J. B., Frank, A., Bjorkman, J. E., Livio, M., 1999, *ApJ*, 512, 322

Ekström S., Georgy, C., Meynet, G., Groh, J., Granada, A., 2013, in Kervella, P., Le Bertre T., Perrin, G., eds, EAS Publications Series Vol. 60, EAS Publications Series. pp 31–41 (`arXiv 1303.1629`), doi:10.1051/eas/1360003

Georgy C., 2012, *A&A*, 538, L8

Georgy, C., Ekström S., 2015, in EAS Publications Series. pp 41–46 (`arXiv 1508.04656`), doi:10.1051/eas/1571007

Georgy, C., Ekström S., Saio, H., Meynet, G., Groh, J., Granada, A., 2013, in Kervella, P., Le Bertre T., Perrin, G., eds, EAS Publications Series Vol. 60, EAS Publications Series. pp 43–50 ( `arXiv 1301.2978`), doi:10.1051/eas/1360004

Groh, J. H., Meynet, G., Ekström S., 2013, *A&A*, 550, L7

Harper, G. M., Richter, M. J., Ryde, N., Brown, A., Brown, J., Greathouse, T. K., Strong, S., 2009, *ApJ*, 701, 1464

Höfner S., 2008, *A&A*, 491, L1

Humphreys, R. M., Helton, L. A., Jones, T. J., 2007, *AJ*, 133, 2716

Jones, T. J., Humphreys, R. M., Helton, L. A., Gui, C., Huang, X., 2007, *AJ*, 133, 2730

Levesque, E. M., Massey, P., Olsen, K. A. G., Plez, B., Josselin, E., Maeder, A., Meynet, G., 2005, *ApJ*, 628, 973

Macintosh, B., *et al.*, 2006, in Society of Photo-Optical Instrumentation Engineers (SPIE) Conference Series. p. 62720L, doi:10.1117/12.672430

Martinache, F., Guyon, O., 2009, in Techniques and Instrumentation for Detection of Exoplanets IV. p. 74400O, doi:10.1117/12.826365

Mathis, J. S., Rumpl, W., Nordsieck, K. H., 1977, *ApJ*, 217, 425

Meynet, G., *et al.*, 2015, *A&A*, 575, A60

Norris, B. R. M., *et al.*, 2012, *Nature*, 484, 220

Ossenkopf, V., Henning, T., Mathis, J. S., 1992, *A&A*, 261, 567

Scicluna, P., Siebenmorgen, R., Wesson, R., Blommaert, J. A. D. L., Kasper, M., Voshchinnikov, N. V., Wolf, S., 2015, *A&A*, 584, L10

Smith, N., 2014, *ARA&A* 52, 487

Smith, N., Humphreys, R. M., Davidson, K., Gehrz, R. D., Schuster, M. T., Krautter, J., 2001, *AJ*, 121, 1111

Su, J. B., Shen, Z.-Q., Chen, X., Yi, J., Jiang, D. R., Yun, Y. J., 2012, *ApJ*, 754, 47

Verhoelst, T., van der Zypen N., Hony, S., Decin, L., Cami, J., Eriksson, K., 2009, *A&A*, 498, 127

Xu, S., Ertel, S., Wahhaj, Z., Milli, J., Scicluna, P., Bertrang, G. H.-M., 2015, *A&A*, 579, L8

van Loon J. T., 2013, in Kervella P., Le Bertre T., Perrin, G., eds, EAS Publications Series Vol. 60, EAS Publications Series. pp 307–316 (`arXiv 1303.0321`), doi:10.1051/eas/1360036

van Loon J. T., Cioni, M.-R. L., Zijlstra, A. A., Loup, C., 2005, *A&A*, 438, 273